Subaqueous sediment gravity flows undergoing progressive solidification

Amiruddin, Hideo Sekiguchi & Shinji Sassa

The flow-out potential of a body of fluidized sediment following abrupt collapse is discussed through numerical and physical modelling. The emphasis of the analysis procedure is placed on considering density stratification that occurs in highly concentrated sediment gravity flows. Specifically, it combines Navier-Stokes/continuity equations for a liquefied soil domain with a consolidation equation for the underlying, progressively solidifying soil domain. Evolutions of the flow and solidification surfaces are traced as part of the solution using a volume-of-fluid (VOF) technique. The physical modelling is concerned with two-dimensional flume tests, together with related fluidization and sedimentation tests under one-dimensional conditions. A body of fluidized sandy sediment was subjected to abrupt collapse and allowed to flow out into ambient water. The observed and calculated results show that the highly concentrated sediment flow manifests itself as a decelerating gravity flow due to interactions between the flowing fluidized sediment and accreting soil with a grain-supported framework being reestablished.

Amiruddin, Geophysics Laboratory, Faculty of Science, Hasanuddin University, Makassar 90245, South Sulawesi, Indonesia; Hideo Sekiguchi, Disaster Prevention Research Institute, Kyoto University, Fushimi-ku, Kyoto 612-8235, Japan. E-mail: sekiguch@ujigawa.mbox.media.kyoto-u.ac.jp; Shinji Sassa, Port and Airport Research Institute, 3-1-1 Nagase, Yokosuka, Japan.

Introduction

Highly concentrated sediment flows may occur following failures of loosely compacted, granular slopes underwater or in waterfront areas. The mobility of such sediment flows is of considerable interest to the integrity of coastal fills, underwater pipelines and other such marine facilities. However, the physics of highly concentrated sediment-water mixtures is complex in nature and calls for more development through fundamental approaches (Shanmugam 1996; Ilstad et al. 2004).

The purpose of this paper is to discuss the performance of density stratification in highly concentrated sandy gravity flows underwater, through physical and analytical modelling. From an analytical point of view, the density stratification requires a consistent treatment of moving boundaries. Also, it requires a physically sound treatment of phase change that occurs upon deposition. Indeed, re-sedimentation during flowage brings about not just an accreting soil layer, but the transformation of the state of sediment upon deposition; namely, fluidized sediment transforms itself into a solid with a grain-supported framework being reestablished. A computational model with these features accounted for will be discussed below in this paper.

From a technical point of view, highly concentrated granular flows pose difficulties in observing evolutions of their internal structure even in the laboratory. Recently, Ilstad et al. (2004) resolved this problem by making use of a particle tracking method, coupled with a high-speed video, in a comprehensive set of subaqueous debris flow experiments. Our experiments using a particle image velocimetry (PIV) seem to be along the same line of research strategy as Ilstad et al. (2004). It is noteworthy here that recognizing the limited field of view of our CCD camera, we carried out a sufficient number of identical sandy gravity flow experiments so as to cover the entire processes of flow initiation, flow deceleration and eventual resedimentation. The experimental performance will subsequently be described, in light of the analytical framework that is workable yet deserves further development.

Numerical model developed

Let us briefly review the features of the analytical framework concerned. Sassa et al. (2003) developed a two-dimensional analysis code, named LIQSEDFLOW, so as to describe liquefied sediment flows undergoing progressive solidification. Progressive solidification is a sort of phase-change process and allows transitory fluid-like particulate sediment to reestablish a grain-supported framework during continued disturbances such as wave loading (Miyamoto et al. 2004). Recently, Amiruddin et al. (2004, 2005) extended LIQSEDFLOW

to facilitate a three-dimensional analysis for gravity flows of fluidized sediment.

Consider a body of subaqueous liquefied soil with a mass density ρ_2 whose value is significantly larger than a mass density ρ_1 of the ambient quiescent water with a depth h (Fig. 1(a)). One of the simplest yet meaningful modelling for the liquefied soil is to regard it as a heavy, incompressible viscous fluid with a distinct flow surface. There follow

$$\frac{\partial v_i}{\partial x_i} = 0\,; \quad \rho_2 \left(\frac{\partial v_i}{\partial t} + v_j \frac{\partial v_i}{\partial x_j} \right) = -(\rho_2 - \rho_1)g_i - \frac{\partial p_e}{\partial x_i} + \mu \frac{\partial}{\partial x_j} \left(\frac{\partial v_i}{\partial x_j} \right) \quad (1)$$

where v_i is the velocity, p_e is the excess porewater pressure which represents the excess in porewater pressure over the hydrostatic water pressure $p_s = \rho_1 g(h-z)$ where $z = x_3$, g_i is the gravitational acceleration with the components $(0,0,g)$, and μ stands for the dynamic viscosity of the liquefied soil. The dynamic viscosity of the transitory fluid-like liquefied sediment may depend on a number of factors, including local particle concentration and shear-induced particle migration (Phillips et al. 1992). In order to keep the present treatment as simple as possible, however, we decided to set the dynamic viscosity in Eq. (1) being numerically equal to that of pure water.

The progress of solidification of the liquefied flow may be effected by three-dimensional consolidation, which reads:

$$\frac{\partial (p_e - \sigma_m)}{\partial t} = \frac{1}{\rho_1} M \cdot K \frac{\partial}{\partial x_j} \left(\frac{\partial p_e}{\partial x_j} \right) + \text{(source term)} \quad (2)$$

where ρ_1 is the density of the ambient fluid, K is the Darcy permeability coefficient, M is the bulk modulus of the soil skeleton and σ_m is the mean total stress of the solidifying particulate sediment.
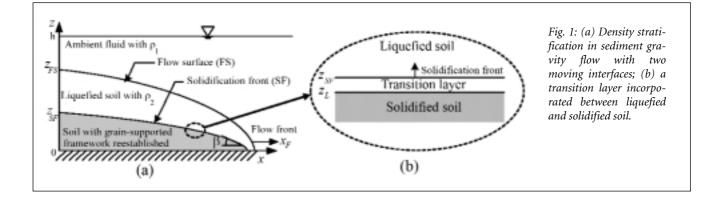
The governing equations are discretized in a non-uniform Eulerian mesh using the MAC finite difference method (Amsden and Harlow 1970). For tracking the flow surface the volume-of-fluid (VOF) technique (Hirt and Nichols 1981) was applied, along with an efficient volume-advection scheme (Hamzah 2001) so

as to ensure the conservation of mass in the course of flowage. The evolution of the interface between the domains of liquefied and solidified soil was also effectively traced using the VOF technique. Specifically, the soil undergoing solidification was treated as being an obstacle to the flowing liquefied soil, such that the velocities in the solidified soil become zero. This assumption is justifiable since the solidified zone should have a much higher stiffness and frictional resistance than the liquefied soil.

A transition layer of "structured liquefied soil" is introduced in such a way that it occupies the lowermost part of the liquefied soil domain and immediately overlies the solidified soil domain (Fig. 1(b)). By doing so, one can realize the phase change that may occur in accordance with the advance of the solidification front. In a computational step, the solidification front may be judged to be an active one if the effective stress increment in the transition layer becomes positive. Then, the solidification front can move upwards by an amount equal to the prescribed thickness of the transition layer. Concurrently, the liquefied soil domain retreats by the same amount, and the transition layer assumes a new (higher) location. The slope of the solidification surface, β, may be modified, if necessary, so as not to exceed a critical angle β_{cr} in view of the frictional resistance of the soil (Fig. 1(a)).

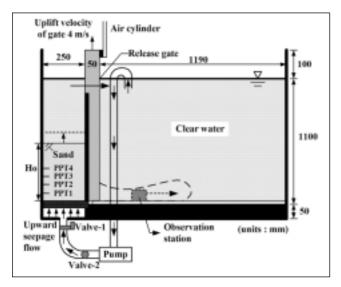# Physical modelling of fluidization, hindered settling and sediment gravity flow

Experimental program and test procedure

The experimental program consisted of (A) three sets of two-dimensional sediment gravity flow tests following fluidization and (B) a set of fluidization and hindered settling tests under one-dimensional conditions. The sand used was silica No. 6 which had an average grain size of 0.32 mm and a mass density of solid particles $\rho_s = 2.65$ g/cm³. The void ratio of the sand in the loosest packing, e_{max}, was equal to 1.17, corresponding
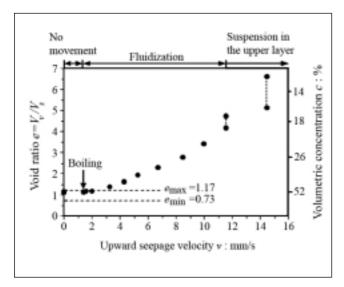

Fig. 1: (a) Density stratification in sediment gravity flow with two moving interfaces; (b) a transition layer incorporated between liquefied and solidified soil.

to the concentration of solids by volume, $c_{lp}= 1/(1+e_{max})$ =46%. Here void ratio e is defined as the volume of the void space, V_v, to the volume of the solid grains, V_s. The void ratio of the sand in the densest packing, e_{min}, was equal to 0.73 with the corresponding volumetric concentration c_{dp}=58%.

The flume used was 1.5 m long, 1.25 m deep and 0.05 m thick (Fig. 2). The depth of ambient water in each test was kept at 1.1m. A sand layer 5mm thick was placed on the floor of the channel in order to achieve realistic boundary conditions for the sediment gravity flow. The sediment was then subjected to upward seepage flow under a given discharge velocity, yielding a liquefied or fluidized state of sediment (Fig. 3). Then, the release gate was swiftly opened, allowing the sediment to flow out over a horizontal floor in the channel.

Fig. 2: Setup for experiment on sediment gravity flow following fluidization.

Fig. 3: Void ratios of sediment plotted against imposed vertical seepage velocities, showing transformation of the state of sediment.

The three sets of gravity flow experiments were performed with relatively high concentrations but smaller than c_{lp}: namely, c=30%; 34%; 38% and 42%. The first series examined the effect of solids concentration upon flow-out potential, with the aid of a high-speed CCD camera (recording rate: 125 frames/s; shutter speed: 1/1000 s and resolution: 640x240 pixels). The second series put emphasis on capturing overall deformed configurations of fluidized sediment by means of a digital video camera (Handycam). In this series, the initial height of the sand deposit, H_0 was set equal to 150mm. The height of fluidized sand, H, was varied to give different concentrations, c. The third series of experiments dealt with the sediments having c=38%. In order to overcome the limited field of view (50mm x 40mm) of the CCD camera used, we performed a total of 24 identical flume tests by varying the CCD-camera position only.

A PIV technique was applied to a range of imagery obtained with the high-speed CCD camera, providing a useful dataset regarding the evolution of the velocity field in the sediment gravity flow. We used a PIV-software named KUpiv_v1 (Kimura et al. 2001) for the image processing. It is based essentially on a cross-correlation pattern matching technique which involves two consecutive images with a time spacing $N\Delta t$. Here we selected Δt equal to 1/125 seconds and N equal to one for sediment gravity flow experiments.

Fluidization and hindered settling

Before going into the discussion of the sediment gravity flow experiments, let us review the experimental performances of fluidization and hindered settling that were obtained under one-dimensional conditions. These tests were performed using the reservoir in the flume with the release gate tightly closed. Four pore-pressure transducers (PPTs) were mounted on the wall of the reservoir (Fig. 2).

Fluidization

The pore pressures in a column of completely fluidized sediment with a constant concentration c should obey the following relation: $P_e=-\gamma'(z-z_{FS})$, since the effective stress there is zero by definition. Here γ' stands for the submerged unit weight of the sediment, $\gamma'=(\rho_s-\rho_w)gc$, and z_{FS} is the elevation of the uppermost surface of the fluidized sand. The time-averaged values of the pore pressures during the fluidization stage in test FEB05-②A-3 are typified in Fig. 4. It is evident in this figure that the data points conform well to the theoretical curve, giving γ'=633 kgf/m³; namely, c=38.4%. It is noteworthy that the value of c is consistent with the value c=38.3% which was obtained from the measurement of the height H of the fluidized sediment column.
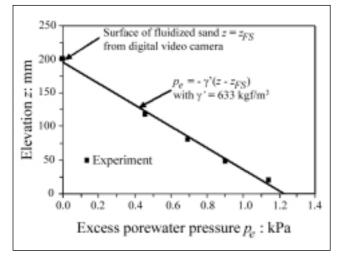
Fig. 4: Profile of excess porewater pressures in fluidized sand column from test FEB05-②A-3 (c = 38 %).

Fig. 5: Temporal changes in the profile of pe against z during resedimentation for test FEB05-②A-3 (c = 38 %).

Hindered settling

When the valve to the water feeding pump was closed, the fluidized sediment started resedimentation. Temporal changes in the profile of pore water pressures P_e against elevation z are shown in Fig. 5. The associated time histories of the flow and solidification surfaces are shown in Fig. 6. The flow surface gradually advanced downwards and reached a level that was very close to the initial surface of the sand deposit. The application of the PIV technique to a total of four identical subtests in test FEB05-②A clearly showed that the solidification front advanced upwards and reached the level very close to the flow surface. The termination of the resedimentation process should be at point B' or slightly beyond. The overall rate of advance of the solidification front, dz_{SF}/dt, was evaluated to be equal to 17 mm/s (slope OB' in Fig. 6).

A summary plot of the measured settling velocities w (e.g., slope AB in Fig. 6) in the sand-water mixtures is presented in Fig. 7 against the concentrations c concerned. For purposes of comparison, the upward seepage velocities that were needed to induce fluidization are also plotted in this figure. It is seen that both of the settling velocity and seepage velocity to induce fluidization tend to decrease with the increases in volumetric concentration, c.

Fig. 6: Evolutions of flow and solidification surfaces in test FEB05-②A (c = 38 %).

Fig. 7: Settling velocities and seepage velocities to induce fluidization plotted against volumetric concentrations of sediment.

Characteristics of subaqueous sediment gravity flow

Overall flow pattern

We observed that the fluidized sediment gravity flow consisted of three regions: 0<z<SF; SF<z<FS and FS<z. The region between the base and solidification front

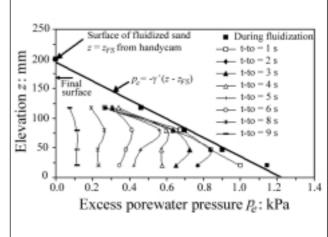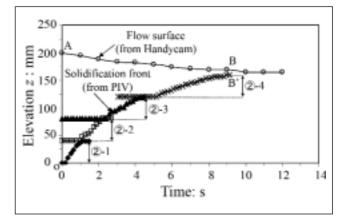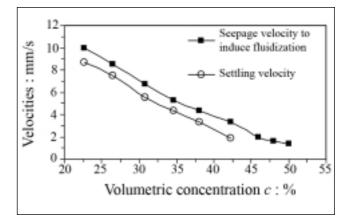(0<z<SF) was the solidification zone in which the sediment had zero velocities, reestablishing a grain-supported framework. In the region SF<z<FS, the highly concentrated sediment flew in non-turbulent regime. In

contrast, the region above the flow surface (FS<z) contained only dilute sediment clouds, the behavior of which appeared to be effected by turbulence and entrainment of ambient water. The performance of the sediment clouds in the region with z >FS is beyond the scope of the following discussion.

The overall flow pattern in sediment gravity flows is typified in Fig. 8 for c=42% and c=38%. These pictures were taken using the digital video camera (Handycam) at a frame rate equal to 1/30 seconds, providing a general idea as to how the gravity flow started and came to the final stage of deposition. More specifically, let us look at the performance in test DVFLOW-2. Upon lift-up of the gate there occurred a vertical dilute sediment stream. However, its influence on the overall flow pattern was judged to be negligible. In the upper three photographs in Fig. 8(b) one may notice the rounded head advancing on the horizontal floor. At an elapsed time of t=2.0s, trains of vortex were seen to form behind the advancing head. The vortex trains featured the region above the main body of the sediment gravity flow (z>FS), thus receiving no further discussion. It is noteworthy in the lowermost photograph of Fig. 8(b) that the sediment gravity flow finally came to a stop, forming a very gentle slope. This aspect will be discussed later in this paper in more detail.

The measured evolutions of the head of the sediment gravity flows are shown in Fig. 9 for the four different volumetric concentrations, c. In this figure, the measured performance of gravity flow of clear water in air is also plotted. It is seen that the gravity flow of clear water exhibited a nearly constant rate of flowage until the flow head hit the downstream end of the channel. By contrast, the sediment gravity flows underwent decelerating flowage, except for the early stage of flow initiation.

Evolutions of flow surface and solidification front
Let us now discuss the measured performance of fluidized sediment gravity flow with c=38% in more detail (Fig. 10). This representation was made possible by performing a total of twenty-four identical flume tests and by assembling pictures taken from the twenty-four differing stations with the single CCD-camera. A close look at Fig. 10 permits one to grasp the evolution of the flow surface of the highly concentrated gravity flow, including the location of the flow head. Also, it provides a comprehensive set of digital data for facilitating the PIV technique to work out the evolution of the internal flow structure.

The identification of the flow surface could be made by visual inspection alone. For instance, let us look at Fig. 11 where four snapshots of sediment gravity flow in test CCDFLOW-11 (c=38%) are shown. Note in this figure that T_a represents the instant of time when the
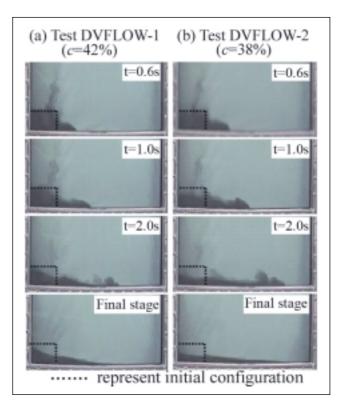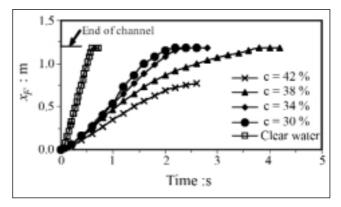

Fig. 8: Photographs of sediment gravity flows with c=42% and c=38%.

Fig. 9: Measured time histories of locations of gravity flow head in second series of experiment.

flow head reached the right end of the station of observation (x=650mm). The flow surface (FS) became apparent 0.48 seconds after the gravity flow head passed the observation station, and thereafter the flow surface became clearer.

On such an individual imagery basis, however, one could not identify the formation of the solidification zone because the body of the highly concentrated sandy flow was, in fact, featureless. As pointed out earlier, the velocity fields obtainable from the PIV technique revealed the formation and development of the solidification front (Fig. 12). In this figure it can be readily seen that the region with zero velocities spread upwards as time elapsed, indicating the occurrence of progressive solidi-
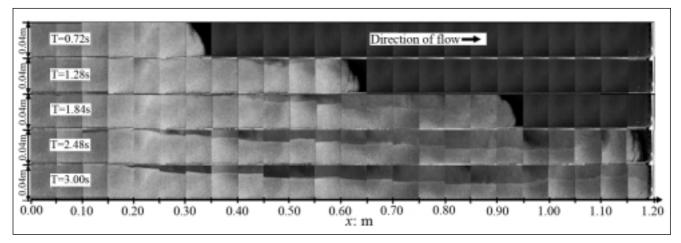
Fig. 10: Flow configurations of initially fluidized sediment with c=38% at five elapsed times indicated.
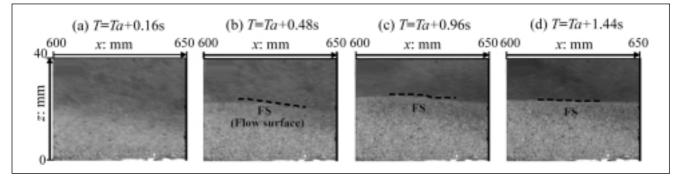

Fig. 11: Snapshots of fluidized sediment gravity flow in test CCDFLOW-11 from a fixed station using the high-speed CCD camera (c = 38 %).
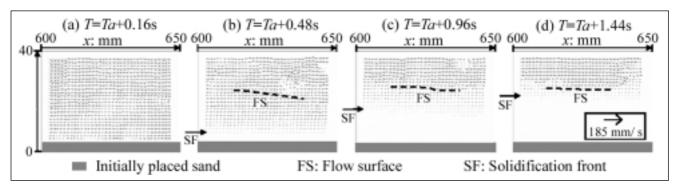

Fig. 12: Velocity fields of sediment gravity flow in test CCDFLOW-11 obtained through PIV technique, showing upward advance of solidification front designated SF (c = 38 %).

fication during flowage. Indeed, the solidification front (SF) is a moving interface between the zones of completely fluidized sediment and accreting soil with a grain-supported framework being reestablished. The velocity profiles obtained for x=624 mm are presented in Fig. 13. Here u and w respectively denote the horizontal and vertical velocities. The way in which the solidification front developed during flowage, may be clearly seen from this figure by noting the evolution of the profile of horizontal velocities.

The layered nature of the sediment gravity flow with c=38% is shown in Fig. 14. It is important here to note

that the flow thickness becomes progressively smaller, thereby making the flowage slow down.

Depositional features

The way in which a sandy gravity-flow deposit was progressively formed, can be clearly seen in Fig. 15. Note in this figure that the deposit made a gentle slope of one in thirty or so, underwent accretion and took the essentially final form at an elapsed time of 3.0 s in this particular experiment. The total volume of the final deposit (at $t = 3.0$s) was evaluated, giving rise to the overall void ratio e equal to 1.11. The e value was only slightly
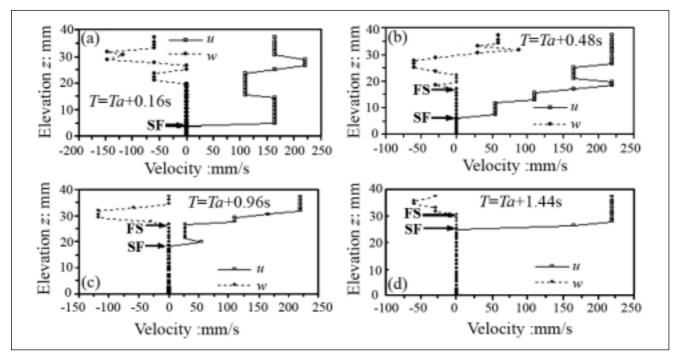
Fig. 13: Profiles of flow velocities at x=624mm with elevation for four different instants of time.

smaller than the e_{max} of 1.17, suggesting the occurrence of the sandy gravity flow in relatively mild conditions. Also, an idea about the deposition rate is obtainable from Fig. 15. In fact, the deposition rate was equal to 10 mm/s or somewhat larger. Note that the deposition rate was much faster than the rate of hindered settling for c=38% (i.e., w_s=3.3 mm/s).
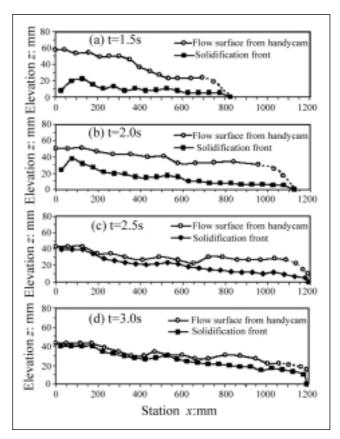
The consideration of conservation of mass permits one to estimate the deposition rate, dz_{SF}/dt, as follows (Lowe 1976):

$$\frac{dz_{SS}}{dt} = \frac{c}{c^* - c} w_s(c) = \frac{0.38}{0.46 - 0.38} \times 3.3 = 15.7 \text{ mm/s} \qquad (3)$$

Here c^* represents the volumetric concentration of the sediment with a grain-supported framework reestablished. It generally is subject to the following inequalities: $c_{lp} \leq c^* \leq c_{dp}$. The reason we simply set $c^*=c_{lp}$ in Eq. (3) derives from the observation that the deposit was in a very loose state of packing. Although the estimated deposition rate was somewhat larger than those observed, it surely emphasizes the importance of further examining the role of hindered settling in the context of sediment gravity-flow dynamics.

Comparison between predicted and measured performances of gravity flows

A series of analyses of gravity flows was performed in conjunction with the experimental program described above. A computational domain, 10 units horizontal by 2.5 units vertical, was discretized into a total of 100 by

Fig. 14: Measured flow configurations at four different times in sediment gravity flow with c=38%.

25 grids. A regular interval, $\Delta X=0.1$, was applied in X-direction, and a variable grid was used in Z-direction with a minimum grid $\Delta Z=0.01$ near the bottom of the
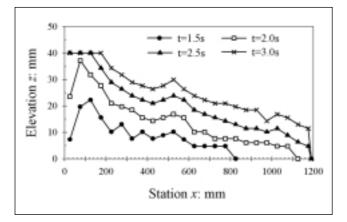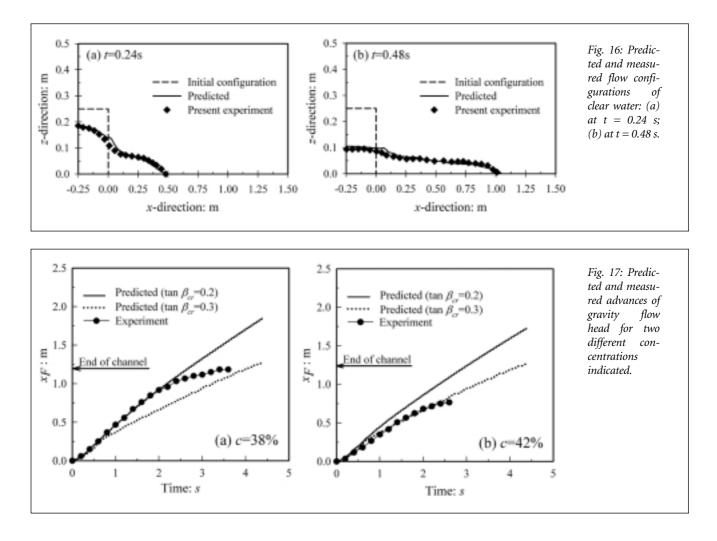
Fig. 15: Locations of solidification front at four different times in sediment gravity flow (c=38%) obtained through PIV technique.

computational domain. The variables used in the computations were all non-dimensional variables by choosing the width of the reservoir, *a=0.25m*, as a reference length and $\sqrt{ga}$ as a reference velocity. Here g denotes the gravitational acceleration and is equal to 9.8m/s². The non-dimensional kinematic viscosity $\nu/(a\sqrt{ga})$ was then equal to 2.6x10⁻⁶; the reciprocal of it

corresponded to Re=3.8x10⁵. The non-dimensional time increment $\Delta T = \Delta t \sqrt{g/a}$ was taken as 0.001. In the problem under discussion a rectangular column of heavy fluid (fluidized soil) was initially confined between a vertical wall and a gate, and was kept in hydrostatic equilibrium. At the beginning of the calculation, the release gate was instantaneously removed and the dense fluid (fluidized soil) in the reservoir was allowed to flow out onto a horizontal floor.

Let us first discuss the abrupt collapse of a column of clear water into ambient air. The predicted changes in the configuration of the column of clear water (*a*=0.25m, *b*=0.25m) are illustrated in Figs. 16, together with the experimental results. Here a and b stand for the width and height of the initial configuration of the water column. It is seen that the predicted performance compares favourably with the observed flow behaviour.

Let us now discuss the performance of sediment gravity flows following fluidization. Only two cases with *c*=38% and *c*=42% are taken up here (Figs. 17). It is seen that in the case with *c*=38% (Fig. 17(a)) the predicted performance with tanβ_{cr}=0.2 compares well with the observed flow behaviour in the early and interme-

Fig. 16: Predicted and measured flow configurations of clear water: (a) at t = 0.24 s; (b) at t = 0.48 s.

Fig. 17: Predicted and measured advances of gravity flow head for two different concentrations indicated.

diate stages of flowage. The observed performance for c=42% in Fig. 17(b) is of particular interest, because the flowage underwent marked deceleration and came to a complete stop. The predicted performance with $\tan\beta_{cr}$=0.3 reproduced the observed flow pattern better than that with $\tan\beta_{cr}$=0.2. However, either prediction could not reproduce the eventual abrupt cessation of the flowage at c=42%.

The examination of the predicted development of the solidification zone made it clear that the solidification front advanced upwards to a limited extent and did not reach the flow surface during the computational period. A key factor for resolving this limitation would be to quantify precisely the effect of hindered settling and to reflect this in the treatment of obstacles and so forth in the computational procedure.

Conclusions

The flow and depositional aspects of highly concentrated, sandy sediment gravity flows underwater have been discussed in terms of physical and numerical modelling. The principal conclusions derived are as follows:

1. The results from the two-dimensional flume tests show that the sediment gravity flows underwent marked decelerating regime, compared with the gravity flows in clear water.
2. The imagery analysis with PIV revealed the formation and development of the solidification front during flowage. The solidification front clearly separated the completely fluidized flow zone from the accreting soil layer with a grain-supported framework being reestablished.
3. Evaluation of the extent of the solidified zone in the case with c=38% showed that the sediment gravity flow underwent re-deposition in relatively mild conditions, thereby leaving the fabric of very loose packing with e = 1.11. The deposit was also featured by a gentle slope of 1 in 30 or so.
4. The observed density stratification in the highly concentrated, sandy gravity flows generally supports the analytical framework of LIQSEDFLOW (Sassa et al., 2003). It is a subject for future studies to extend LIQSEDFLOW for treating sediment gravity flows on slopes.

References:

Amiruddin, Sassa, S. & Sekiguchi, H. 2004: Analysis of three-dimensional sediment gravity flows. *Annuals, Disaster Prevention Research Institute, Kyoto University* 47B, 617-633.

Amiruddin, Sassa, S. & Sekiguchi, H. 2005: Modelling of sediment gravity flows with progressive solidification. *Annuals, Disaster Prevention Research Institute, Kyoto University* 48B, 757-774.

Amsden, A.A. & Harlow, F.H. 1970: A simplified MAC technique for incompressible fluid flow calculations. *Journal of Computational Physics* 6, 322-325.

Hamzah, M.A. 2001: Numerical simulations of tsunami pressure acting upon coastal barriers on wet and dry lands. Doctoral thesis, *Graduate School of Engineering, Kyoto University*.

Hirt, C. W. & Nichols, B. D. 1981: Volume of fluid (VOF) method for the dynamics of free boundaries. *Journal of Computational Physics* 39, 201-225.

Ilstad, T., Elverhøi, A. Issler, D. & Marr, J. G. 2004: Subaqueous debris flow behaviour and its dependence on the sand/clay ratio: a laboratory study using particle tracking. *Marine Geology* 213, 415-438.

Kimura, I., Uemura, T. & Okuno, T. 2001: Visualization Techniques. *Kindai-kagaku-sha Publishing* (in Japanese).

Lowe, D.R. 1976: Subaqueous liquefied and fluidized sediment flow and their deposits. *Sedimentology* 23, 285–308.

Miyamoto, J., Sassa, S. & Sekiguchi, H. 2004: Progressive solidification of a liquefied sand layer during continued wave loading, *Geotechnique* 54, 617-629.

Phillips, R.J., Armstrong, R.C., Brown, R.A., Graham, A.L. & Abbot, J.R. 1992: A constitutive equation for concentrated suspensions that account for shear-induced particle migration. *Physics of Fluids* A4, 30-40.

Sassa, S., Miyamoto, J. & Sekiguchi, H. 2003: The dynamics of liquefied sediment flow undergoing progressive solidification. *In* J. Locat and J. Mienert (Eds.), *Submarine Mass Movements and Their Consequences*, Kluwer Academic Publishers, 95-102.

Shanmugam, G. 1996: High-density turbidity currents: are they sandy debris flows? *Journal of Sedimentary Research* 46, 2-10.